



THE UNIVERSITY *of* EDINBURGH

Edinburgh Research Explorer

Pro-death NMDA receptor signaling is promoted by the GluN2B C-terminus independently of Dapk1

Citation for published version:

McQueen, J, Ryan, TJ, McKay, S, Marwick, K, Baxter, P, Carpanini, SM, Wishart, TM, Gillingwater, TH, Manson, JC, Wyllie, DJA, Grant, SGN, McColl, BW, Komiyama, NH & Hardingham, GE 2017, 'Pro-death NMDA receptor signaling is promoted by the GluN2B C-terminus independently of Dapk1', *eLIFE*, vol. 2017, no. 6, e17161. <https://doi.org/10.7554/eLife.17161>

Digital Object Identifier (DOI):

[10.7554/eLife.17161](https://doi.org/10.7554/eLife.17161)

Link:

[Link to publication record in Edinburgh Research Explorer](#)

Document Version:

Peer reviewed version

Published In:

eLIFE

General rights

Copyright for the publications made accessible via the Edinburgh Research Explorer is retained by the author(s) and / or other copyright owners and it is a condition of accessing these publications that users recognise and abide by the legal requirements associated with these rights.

Take down policy

The University of Edinburgh has made every reasonable effort to ensure that Edinburgh Research Explorer content complies with UK legislation. If you believe that the public display of this file breaches copyright please contact openaccess@ed.ac.uk providing details, and we will remove access to the work immediately and investigate your claim.



1
2 **Pro-death NMDA receptor signaling is promoted by the GluN2B C-terminus**
3 **independently of Dapk1**
4

5 Jamie McQueen^{1,2#}, Tomás J. Ryan^{3#}, Sean McKay^{2#}, Katie Marwick², Paul Baxter^{1,2}, Sarah M.
6 Carpanini^{4,5}, Thomas M. Wishart^{4,5}, Thomas H. Gillingwater^{1,5}, Jean C. Manson^{4,5}, David J. A.
7 Wyllie¹, Seth G. N. Grant^{6,7}, Barry McColl^{1,4*}, Noboru H. Komiyama^{6,7*} and Giles E. Hardingham^{1,2,5*}
8
9
10

11 ¹ UK Dementia Research Institute at the University of Edinburgh, Edinburgh Medical School,
12 University of Edinburgh, Edinburgh, EH8 9XD, UK.

13 ²Centre for Discovery Brain Sciences, University of Edinburgh, Hugh Robson Building, George
14 Square, Edinburgh EH8 9XD, UK.

15 ³School of Biochemistry and Immunology, Trinity College Dublin, 152-160 Pearse Street Dublin 2,
16 Ireland

17 ³Howard Hughes Medical Institute, Massachusetts Institute of Technology, Cambridge, MA 02139,
18 USA

19 ⁴The Roslin Institute, University of Edinburgh, Easter Bush. Midlothian EH25 9RG, UK

20 ⁵nPAD MRC Mouse consortium, University of Edinburgh

21 ⁶Wellcome Trust Sanger Institute, Hinxton CB10 1SA, UK

22 ⁷Centre for Clinical Brain Sciences & Centre for Neuroregeneration, University of Edinburgh
23 Chancellor's Building, Edinburgh, CB10 1SA, UK.
24
25
26
27
28

29 #Equal contribution
30

31 * Correspondence to Giles E. Hardingham (Giles.Hardingham@ed.ac.uk), Noboru H. Komiyama
32 (N.Komiyama@ed.ac.uk) or Barry McColl (Barry.McColl@roslin.ed.ac.uk)
33
34
35
36
37

38

39 **Abstract**

40 Aberrant NMDA receptor (NMDAR) activity contributes to several neurological disorders, but direct
41 antagonism is poorly tolerated therapeutically. The GluN2B cytoplasmic C-terminal domain (CTD)
42 represents an alternative therapeutic target since it potentiates excitotoxic signaling. The key
43 GluN2B CTD-centred event in excitotoxicity is proposed to involve its phosphorylation at Ser-1303
44 by Dapk1, that is blocked by a neuroprotective cell-permeable peptide mimetic of the region.
45 Contrary to this model, we find that excitotoxicity can proceed without increased Ser-1303
46 phosphorylation, and is unaffected by Dapk1 deficiency *in vitro* or following ischemia *in vivo*.
47 Pharmacological analysis of the aforementioned neuroprotective peptide revealed that it acts in a
48 sequence-independent manner as an open-channel NMDAR antagonist at or near the Mg²⁺ site,
49 due to its high net positive charge. Thus, GluN2B-driven excitotoxic signaling can proceed
50 independently of Dapk1 or altered Ser-1303 phosphorylation.

51

52

53 Introduction

54 NMDA receptor (NMDAR) -mediated excitotoxicity plays a key role in acute neurological disorders
55 such as stroke and traumatic brain injury, neuronal loss in Huntington's disease, and is also
56 implicated in synapto-toxicity in Alzheimer's disease ¹⁻⁷. Most NMDARs are comprised of two
57 obligate GluN1 subunits and two GluN2 subunits ⁸, with GluN2A and GluN2B predominant in the
58 forebrain ⁹⁻¹³. GluN2 subunits have long, evolutionarily divergent cytoplasmic C-terminal domains
59 (CTDs) which we have shown can differentially associate with signalling molecules ¹⁴⁻¹⁷ and
60 differentially signal to cell death: the CTD of GluN2B (CTD^{2B}) potentiates excitotoxicity more
61 strongly than that of GluN2A ¹⁴.

62 While multiple pathways contribute to excitotoxicity ¹⁸, the mechanism by which CTD^{2B} is
63 thought to potentiate excitotoxicity is upstream of all of them ^{6,19,20}. The mechanism is centred on
64 Ser-1303 of CTD^{2B}, within a region of the CTD unique to GluN2B, and with which CaMKII α is known
65 to interact and phosphorylate ^{21,22}. It was reported that in response to ischemia or excitotoxic insults,
66 a different kinase, Dapk1, causes Ser-1303 phosphorylation which increases NMDAR-dependent
67 ionic flux ¹⁹. Consistent with this, *Dapk1*^{-/-} neurons were reported to be resistant to excitotoxicity, and
68 a cell-permeable peptide mimetic of the CTD^{2B} region around Ser-1303 disrupted Ser-1303
69 phosphorylation and was neuroprotective ¹⁹.

70 Given that the GluN2B-Dapk1 pathway is prominent in contemporary models of excitotoxicity
71 ^{6,20} we sought to investigate this pathway further. Dapk1 has not hitherto emerged from proteomic
72 post-synaptic density screens ²³⁻³⁰, and we failed to detect it in a recent proteomic analysis of native
73 NMDAR supercomplexes ¹⁷. Moreover, the use of cell-permeable peptides to draw wide-ranging
74 mechanistic conclusions can be problematic without extensive controls. We investigated whether
75 Dapk1-mediated Ser-1303 phosphorylation indeed represents the major reason why CTD^{2B}
76 promotes excitotoxicity signaling better than CTD^{2A}, using approaches that include analysis of a
77 new Dapk1 knockout mouse and the generation of a knock-in mouse with a targeted phospho-
78 mimetic mutation of the CAMKII α /putative Dapk1 interaction site.

79

80 Results

81 Excitotoxic insults do not induce GluN2B Ser-1303 phosphorylation

82 We first examined the influence of excitotoxic conditions on GluN2B Ser-1303 phosphorylation in
83 cortical neurons using a phospho-(Ser-1303)-specific antibody (Millipore 07-398), previously used
84 and validated by several groups ³¹⁻³³.

85 We confirmed that the antibody is capable of detecting changes in Ser-1303 phosphorylation
86 in neurons: phospho-GluN2B(Ser-1303) levels in cortical neurons, as assayed by western blot using
87 this antibody, are lowered after incubation of cortical neurons with the general kinase inhibitor
88 staurosporine, and increased modestly by a cocktail of phosphatase inhibitors okadaic acid and FK-
89 506 (Figure 1–figure supplement 1a,b, Figure 1–source data 4). As further evidence of specificity,
90 we found that the antibody completely failed to react with GluN2B in which we had engineered

91 mutations (L1298A/R1300N/S1303D) into the site for a separate study (Figure 1–figure supplement
92 1c,d).

93 We found that bath application of NMDA at excitotoxic concentrations failed to induce
94 significant Ser-1303 phosphorylation (Figure 1a,1b, Figure 1–source data 1). At the late timepoint
95 (60 min, 50 μ M NMDA) we observed a decline in Ser-1303 phosphorylation (Figure 1a,b, Figure 1–
96 figure supplement 1e,f, Figure 1–source data 5) as well as a decline in total levels of GluN2B,
97 consistent with observations of others who have reported partial calpain-mediated cleavage and
98 degradation of the NMDAR CTD^{34,35}. These observations in DIV10 cortical neurons were also
99 repeated at DIV16 (Figure 1–figure supplement 1g,h, Figure 1–source data 6). We also saw no
100 increase in Ser-1303 phosphorylation in response to oxygen-glucose deprivation (OGD) (Figure
101 1c,d, Figure 1–source data 2), contrary to previous reports¹⁹.

102 To determine whether Dapk1 plays any role in the GluN2B Ser-1303 phosphorylation status,
103 we obtained a *Dapk1*^{-/-} mouse line, created by the International Mouse Phenotyping Consortium by
104 targeted deletion of exon 4 on a C57Bl/6 background (the same strain as the *Dapk1*^{-/-} mouse
105 generated by Tu et al (2010)). The mice had normal fertility, viability and body weight
106 (<http://www.mousephenotype.org>, MGI:1916885). We confirmed that *Dapk1*^{-/-} neurons expressed no
107 Dapk1 (Figure 1e). We compared GluN2B phospho-Ser-1303 levels in cortical neurons obtained
108 from *Dapk1*^{-/-} and *Dapk1*^{+/+} littermates and found no difference in basal levels, nor any difference in
109 the lowered level that we observe at longer periods of NMDA exposure (Figure 1e,f, Figure 1–
110 source data 3). Thus in our hands, Dapk1 does not influence GluN2B Ser-1303 phosphorylation
111 status under basal or excitotoxic conditions.

112

113 **Excitotoxic and ischemic neuronal death can proceed independently of Dapk1**

114 We next addressed the more general point of the role of Dapk1 in excitotoxic neuronal death.
115 Compared to cortical neurons cultured from their wild-type littermates, we observed no difference in
116 NMDAR-dependent excitotoxic neuronal death in *Dapk1*^{-/-} neurons at either DIV10 or DIV16 (Figure
117 2a, Figure 2–source data 1; Figure 2b, Figure 2–source data 2) and no difference in OGD-induced
118 neuronal death (Figure 2c, Figure 2–source data 3), contrary to previous reports. NMDAR currents
119 were also no different in *Dapk1*^{-/-} vs. *Dapk1*^{+/+} neurons (Figure 2d, Figure 2–source data 4).

120 We then studied the influence of Dapk1 deficiency on ischemic neuronal death *in vivo*. We
121 employed a model of transient global ischemia model (bilateral common carotid artery occlusion)
122 used previously to show a protective effect of Dapk1 deficiency¹⁹. Adult mice exposed to a transient
123 (20 min) period of global ischemia showed characteristic selective neuronal death within the
124 hippocampus, particularly the CA1 and CA2 regions. However, *Dapk1*^{-/-} and *Dapk1*^{+/+} mice exhibited
125 similar levels of infarction (Figure 2e-h, Figure 2–source data 5), contrary to previous reports¹⁹.
126 These observations collectively indicate that excitotoxic and ischemic neuronal death *in vitro* and *in*
127 *vivo* can proceed normally in the absence of Dapk1.

128

129
130
131
132
133
134
135
136
137
138
139
140
141
142
143
144
145
146
147
148
149
150
151
152
153
154
155
156
157
158
159
160
161
162
163
164
165
166

TAT-NR2B_{CT} is a direct NMDAR antagonist

In support of the Dapk1 hypothesis for CTD^{2B}-derived excitotoxicity, a cell-permeable (TAT-fused) peptide mimetic of the GluN2B amino acids 1292-1304 (TAT-KKNRNKLRRQHSY: TAT-NR2B_{CT}) was reported to prevent NMDAR-dependent GluN2B Ser-1303 phosphorylation, and excitotoxicity¹⁹. We observed that 50 μM TAT-NR2B_{CT}, the concentration used previously¹⁹, was toxic to neurons (Figure 3–figure supplement 1a, Figure 3–source data 4), so we used a concentration 10 times lower (5 μM). We found that 5 μM TAT-NR2B_{CT} completely prevents NMDA-induced excitotoxicity (Figure 3–figure supplement 1b, Figure 3–source data 5). This was surprising, given that we did not see a role for Dapk1 in excitotoxicity (Figure 2). However, further analysis revealed the explanation: at 5 μM, TAT-NR2B_{CT} potently inhibited NMDAR currents, acting immediately and without any need for a preincubation period (Figure 3a-d, Figure 3–source data 1), and in a manner that was not readily washed out upon removal of peptide (data not shown). TAT-NR2B_{CT} was custom synthesized for our studies by Genscript, and we found that NR2B_{CT}(1292-1304)-TAT, a pre-made peptide sold by Merck Millipore was a similarly potent NMDAR antagonist (n=8, Figure 3–figure supplement 1c). A scrambled version of TAT-NR2B_{CT} (TAT-sNR2B_{CT}) was similarly neuroprotective and similarly antagonistic at the NMDAR (Figure S3b, Figure 3a-d). One potential explanation for the NMDAR antagonistic properties of TAT-NR2B_{CT} is the high positive charge of the peptide (+15 at neutral pH). To investigate this, we designed an arginine-rich peptide of high net positive charge (+15-same as TAT-NR2B_{CT}) of sequence: RRR TQN RRN RRT SRQ NRR RSR RRR) which strongly antagonized NMDAR currents, and another peptide of net neutral charge (NIN IHD VKV LPG GMI KSN DGP PIL), which had a much weaker effect (Figure 3a, Figure 3–source data 1). Taken together these data suggest that the net positive charge of TAT-NR2B_{CT} is primarily responsible for its NMDAR-antagonistic properties. We hypothesized that TAT-NR2B_{CT} may be an open channel blocker drawn partly into the pore by its high net positive charge and bind near the internal Mg²⁺ binding site. Consistent with this, the presence of Mg²⁺ (a pore blocker) reduced the effectiveness of TAT-NR2B_{CT}'s antagonism (Figure 3e, Figure 3–source data 2). Another prediction of this hypothesis is that TAT-NR2B_{CT} would be more effective at antagonising NMDARs under open-channel conditions. To test this, NMDAR currents were measured, after which neurons were incubated in TAT-NR2B_{CT} (5 μM) for 60 s in the presence of zero glycine+100 μM AP5 ("block (1)") to ensure minimal channel opening (closed channel conditions). 60 s was chosen because under conditions of NMDAR agonism this is sufficient time to achieve maximal blockade. After 60 s, both TAT-NR2B_{CT} and AP5 were removed from the bathing medium and NMDAR currents were subsequently re-measured (150 μM NMDA + 100 μM glycine, zero Mg²⁺). The very slow off-rate of the TAT-NR2B_{CT} enabled the peptide's effects on currents to be measured in the absence of the peptide in the medium. TAT-NR2B_{CT} was then applied for a second 60 s ("block (2)") either under the same "closed channel conditions" or under "open channel conditions" (100 μM glycine, 150 μM

167 NMDA). After 60 s TAT-NR2B_{CT} was removed from the bathing medium and NMDAR currents
168 measured for a 3rd time. The NMDAR current remaining at the 2nd and 3rd measurements was
169 calculated as a fraction of the initial current. We found that the 2nd peptide incubation (block (2))
170 significantly increased the proportion of NMDAR inhibition when it occurred under open-channel
171 conditions, but not under closed channel conditions (Figure 3f, Figure 3—source data 3, further
172 evidence in favour of a pore-centred binding site for TAT-NR2B_{CT}. Thus, the unintended NMDAR
173 antagonistic properties TAT-NR2B_{CT} explain its anti-excitotoxic effects.

174

175 Discussion

176 Dapk1-mediated GluN2B Ser-1303 phosphorylation, and consequent enhancement of toxic Ca²⁺
177 influx through extrasynaptic NMDARs lies at the heart of current models of excitotoxicity and of the
178 central role of the GluN2B CTD in this process ^{6,20}, but our study suggests that this needs to be re-
179 appraised. Our observations regarding the (lack of) impact of Dapk1 gene deletion on neuronal
180 vulnerability to excitotoxic and ischemic conditions is at odds with previous reports ¹⁹. The *Dapk1*^{-/-}
181 mouse that we used was generated independently of the one generated by Tu et al., although there
182 is no *a priori* reason why the two lines should behave differently at this fundamental level,
183 particularly given the very similar genetic background (C57BL/6).

184 The potent inhibition of NMDAR currents by TAT-NR2B_{CT} at a concentration up to 100 times
185 lower than that used previously ¹⁹ suggests a simple explanation for its neuroprotective effects
186 independent of Dapk1. We are unable to explain why we observed similar effects of TAT-NR2B_{CT}
187 and its scrambled version, while a selective effect of TAT-NR2B_{CT} was previously reported ¹⁹. Both
188 scrambled versions employed had identical sequences, and the potent NMDAR antagonistic
189 properties of our scrambled peptide are consistent with its neuroprotective properties.

190 One outstanding question is the basis for the modestly reduced excitotoxicity in young
191 neurons when NMDARs lack the GluN2B CaMKII site. We know that NMDAR currents are
192 unaffected, as is the proportion of NMDARs at synaptic vs. extrasynaptic sites, an important factor
193 in excitotoxicity ³⁶, are unaltered. This is consistent with other studies which have concluded that
194 mutation of this site does not affect NMDAR biophysical properties ^{37,38}. More generally, the basis
195 for CTD^{2B}-mediated excitotoxicity ¹⁴ remains incompletely understood. Exchanging the CTD of
196 GluN2B with that of GluN2A by targeted exon exchange reduces vulnerability to excitotoxicity ¹⁴,
197 and performing the reciprocal swap increases vulnerability (SM and GEH, unpublished
198 observations), strongly supportive of a key role for CTD^{2B}. An ongoing avenue of investigation is
199 focussed on understanding the extent to which the composition of the native NMDAR signaling
200 complex is altered by manipulating the endogenous GluN2 CTDs in our panel of knock-in mice. We
201 hypothesize that alterations to the complex may disturb signaling to pro-death events such as NO
202 production, NADPH oxidase activation, oxidative stress, calpain activation and mitochondrial Ca²⁺
203 overload ^{6,20,36,39-43}. Of note, we recently showed that the CTD of GluN2B (as opposed to that of
204 GluN2A) is critically required for formation of 1.5 MDa NMDAR supercomplexes ¹⁷. Thus, regions

205 unique to GluN2B (of which the CaMKII site is one) play a role in higher order signal complex
206 assembly and this may underlie the key role of CTD^{2B} in downstream excitotoxicity¹⁴.

207

208 **Materials and Methods**

209

210 ***Neuronal culture, Dapk^{-/-} mice, induction of excitotoxicity and oxygen-glucose deprivation***

211 Cortical mouse neurons were cultured as described⁴⁴ at a density of between 9-13 x 10⁴ neurons
212 per cm² from E17.5 mice with Neurobasal growth medium supplemented with B27 (Invitrogen,
213 Paisley, UK). Stimulations of cultured neurons were done in most cases after a culturing period of 9-
214 11 days during which neurons develop a network of processes, express functional NMDA-type and
215 AMPA/kainate-type glutamate receptors, and form synaptic contacts. Other experiments were
216 performed at DIV 16. Dapk^{-/-} mice (colony name: H-Dapk1-B11-TM1B, MGI Allele Name:
217 Dapk1tm1b(EUCOMM)Hmgu, RID:MGI:5756958) were generated by MRC Harwell from targeted
218 ES cells made by The European Conditional Mouse Mutagenesis Program, as part of the
219 International Mouse Phenotyping Program. Dapk^{-/-} genotyping reactions were performed using the
220 following primers: A = 5-AGAGAACTGAGGCACCTGG -3', B =, 5'-
221 CATCCAAAGTCCACAGCCAC-3', C=5'-CCAGTTGGTCTGGTGTCA-3' Primer pair A-B recognised
222 the wild-type allele and amplified a product of 322 bp. Primer pair B-C recognised the mutant allele
223 corresponding to a product of 468 bp. PCR reactions were performed using the following cycling
224 conditions: 15 min at 95°C; 36 cycles of 45 s at 94°C, 45 s at 60°C and 1 min at 72°C; and 10 min at
225 72°C.

226 To apply an excitotoxic insult, neurons were first placed overnight into a minimal defined
227 medium⁴⁵ containing 10% MEM (Invitrogen), 90% Salt-Glucose-Glycine (SGG) medium⁽⁴⁶⁾; SGG:
228 114 mM NaCl, 0.219 % NaHCO₃, 5.292 mM KCl, 1 mM MgCl₂, 2 mM CaCl₂, 10 mM HEPES, 1 mM
229 Glycine, 30 mM Glucose, 0.5 mM sodium pyruvate, 0.1 % Phenol Red; osmolarity 325 mosm/l,⁴⁷).
230 Where used, TAT-NR2B_{CT} or TAT-sNR2B_{CT} (5 μM) was incubated for 1h prior to the excitotoxic
231 insult. Neurons were then treated with NMDA (Tocris Bioscience, Bristol, UK) at the indicated
232 concentrations for 1 h, after which medium was changed to NMDA-free. After a further 23 h,
233 neurons were fixed and subjected to DAPI staining and cell death quantified by counting (blind) the
234 number of shrunken, pyknotic nuclei as a percentage of the total. To induce oxygen-glucose
235 deprivation, a previously described approach was used^{48,49}. Briefly, cells were washed and
236 incubated in glucose-free SGG (see formulation above, but with glucose replaced by mannitol) that
237 had been previously degassed with 95% N₂-5% CO₂. The cells were then placed in an anoxic
238 modular incubator chamber for 120 min (as compared to cells washed and incubated in normoxic
239 glucose-containing SGG). For analysis of excitotoxicity, approximately 800-1000 cells were
240 analysed per condition, per replicate (repeated across several replicates), the observer blind to
241 genotype and experimental condition.

242

243 ***Electrophysiological recording and analysis***

244 Coverslips containing cortical neurons were transferred to a recording chamber perfused (at a flow
245 rate of 3-5 ml/min) with an external recording solution composed of (in mM): 150 NaCl, 2.8 KCl, 10
246 HEPES, 2 CaCl₂, 1 MgCl₂, 10 glucose and 0.1 glycine, pH 7.3 (320-330 mOsm). Patch-pipettes
247 were made from thick-walled borosilicate glass (Harvard Apparatus, Kent, UK) and filled with a K-
248 gluconate-based internal solution containing (in mM): potassium gluconate 141, NaCl 2.5, HEPES
249 10, EGTA 11; pH 7.3 with KOH). Electrode tips were fire-polished for a final resistance ranging
250 between 4-8 MΩ. Currents were recorded at room temperature (21 ± 2°C) using an Axopatch 200B
251 amplifier (Molecular Devices, Union City, CA). Neurons were voltage-clamped at -60 mV or +40 mV
252 as indicated, and recordings were rejected if the holding current was greater than -100 pA (-60 mV
253 only) or if the series resistance drifted by more than 20% of its initial value (<25 MΩ). All NMDA
254 currents were evoked by 150 μM NMDA + 100 μM glycine except figure 2D where 50μM NMDA +
255 100 μM glycine was used. Whole-cell currents were analyzed using WinEDR v3.2 software (John
256 Dempster, University of Strathclyde, UK). The approximate number of cells to be recorded was
257 estimated in order to detect a 25% difference in the parameter under study, powered at 80%, based
258 on the standard deviation of data previously published by the laboratory ^{14,50,51}.

259 To determine the ifenprodil-sensitivity of neurons, whole cell NMDA currents were recorded
260 (as described above) followed by the inclusion of 3 μM ifenprodil in the recording solution for a
261 blocking period of 90 seconds. The whole cell NMDA current was the re-assessed, with 3 μM
262 ifenprodil included, and the percentage block calculated. A similar protocol was used to determine
263 the competing effect of Mg²⁺ and TAT-NR2B_{CT} except a blocking period of 60 seconds was used
264 and TAT-NR2B_{CT} was not included when NMDA currents were re-assessed; this may have led to a
265 small washout but we deemed this as negligible due to the slow-off rate of NR2BCT. The
266 membrane potential-dependency of TAT-NR2B_{CT}-induced NMDAR antagonism was determined by
267 applying the peptide for 50-60 seconds after initial steady state at both - 60mV or + 40 mV.

268 To investigate the use dependency of TAT-NR2B_{CT}, we minimized the possibility of the
269 NMDAR channel opening by spontaneous release of glutamate by removing glycine from the ACSF
270 and co-applying 100 μM AP5. Glycine was added back to the ACSF to measure NMDA currents
271 and to facilitate the block of TAT-NR2B_{CT} in the open channel configuration.

272

273 ***Western blotting***

274 Western blotting was performed as described ⁵². In order to minimize the chance of post-
275 translational modifications during the harvesting process, neurons were lysed immediately after
276 stimulation in 1.5x LDS sample buffer (NuPage, Life Technologies) and boiled at 100°C for 10 min.
277 Approximately 10 μg of protein was loaded onto a precast gradient gel (4-16%) and subjected to
278 electrophoresis. Western blotting onto a PVDF membrane was then performed using the Xcell
279 Surelock system (Invitrogen) according to the manufacturer's instructions. Following the protein
280 transfer, the PVDF membranes were blocked for 1 h at room temperature with 5% (w/v) non-fat

281 dried milk in TBS with 0.1% Tween 20. The sample size was calculated based on previous
282 experimental observations of reporting the effect and standard deviation of NMDA-induced Ser-
283 1303 phosphorylation¹⁹. The membranes were incubated at 4°C overnight with the primary
284 antibodies diluted in blocking solution: Anti phospho-(Ser-1303) GluN2B (1: 2000, Millipore), anti-
285 Dapk1 (1:8000, Sigma), anti-GluN2B (C-terminus, 1:8000, BD Transduction Laboratories), anti-beta
286 actin (1:200000, Abcam). For visualisation of Western blots, HRP-based secondary antibodies were
287 used followed by chemiluminescent detection on Kodak X-Omat film. Western blots were digitally
288 scanned and densitometric analysis was performed using Image J. All analysis of GluN2B
289 phosphorylation was normalized to total GluN2B.

290

291 ***Bilateral common carotid artery occlusion***

292 Mice were housed in individually-ventilated cages (in groups of up to five mice) under specific
293 pathogen-free conditions and standard 12 h light/dark cycle with unrestricted access to food and
294 water. All experiments using live animals were conducted under the authority of UK Home Office
295 project and personal licences and adhered to regulations specified in the Animals (Scientific
296 Procedures) Act (1986) and Directive 2010/63/EU and were approved by both The Roslin Institute's
297 and the University of Edinburgh's Animal Welfare and Ethics Committees. Experimental design,
298 analysis and reporting followed the ARRIVE guidelines (<https://www.nc3rs.org.uk/arrive-guidelines>)
299 where possible. The sample size was calculated based on the experimental observations of
300 reporting the effect and standard deviation of BCCAO-induced neuronal loss in both wild-type and
301 *Dapk1*^{-/-}¹⁹, whose experimental observations using n=7 per genotype we retrospectively calculated
302 were powered at >99%.

303 Transient bilateral common carotid artery occlusion (BCCAO) was performed in *Dapk1*^{-/-}
304 and wild-type male control mice under isoflurane anaesthesia (with O₂ and N₂O). The operator was
305 unaware of genotype. Core body temperature was maintained at 37 ± 0.5°C throughout the
306 procedure with a feedback controlled heating blanket (Harvard Apparatus, UK). Both common
307 carotid arteries were exposed and dissected from surrounding tissues and occluded by application
308 of an aneurysm clip for 20 min. Clips were removed, the neck wound sutured and topical local
309 anaesthetic (lidocaine/prilocaine) was applied. Mice were recovered on a heated blanket for 4-6h
310 and then returned to normal housing. After a 3 day recovery, mice were anaesthetised and perfused
311 transcardially with saline followed by 4% paraformaldehyde. Brains were removed and rostral and
312 caudal blocks prepared using a brain matrix (Harvard Apparatus). Blocks were post-fixed in 4%
313 paraformaldehyde for 24 h and processed to paraffin blocks. Sections (6µm) were cut on a
314 microtome (Leica) and stained with haematoxylin and eosin. Ischaemic neuronal death was
315 quantified in the CA1 and CA2 regions of the hippocampus which are the most sensitive regions in
316 this model. Ischaemic (dead) neurons were identified morphologically in two regions of interest
317 (ROIs) in CA1 and the entire CA2 bilaterally. Data are expressed as the number of dead neurons as

318 a % of total neurons in the ROI and show the mean of both hemispheres for each region. All
319 processing and analysis was performed with the operator blind to genotype.

320

321 **Statistical analysis, equipment and settings.**

322 Statistical testing involved a 2-tailed paired Student's t-test, or a one- or two-way ANOVA followed
323 by an appropriate post-hoc test, as indicated in the legends. Cell death analyses for both *in vitro*
324 and *in vivo* experiments were performed blind to the genotype/experimental condition. For all cell
325 death, western blot analyses and *in vitro* and *in vivo* cell death experiments, the value of 'N' was
326 taken as the number of independent biological replicates, defined as independently performed
327 experiments on material derived from different animals. For western blots, we used
328 chemiluminescent detection on Kodak X-Omat film, and linear adjustment of brightness/contrast
329 applied (Photoshop) equally across the image, maintaining some background intensity. In any
330 cases where lanes from non-adjacent lanes are spliced together, lanes are always from the same
331 blot, processed in the same way, and the splicing point is clearly marked. Pictures of cells were
332 taken on a Leica AF6000 LX imaging system, with a DFC350 FX digital camera.

333

334 **Acknowledgements**

335 We thank Michelle Stewart, Roland Quinney and the team at MRC Harwell, the wider International
336 Mouse Phenotyping Consortium, and the MRC Neurodegenerative Processes of Ageing and
337 Disease (nPAD) mouse network for the generation, supply and import of *Dapk^{-/-}* mice. We also
338 thank Kathryn Elsegood and David Fricker for mouse colony management and genotyping. This
339 work is funded by the MRC, Alzheimer's Research UK, Alzheimer's Society, the BBSRC (Roslin
340 Institute strategic programme grant - BB/J004332/1), the Wellcome Trust and the European
341 Commission.

342

343 **Ethics**

344 Animal experimentation: Animals used in this study were treated in accordance with UK Animal
345 Scientific Procedures Act (1986) and the work subject to local ethical review approval by the
346 University
347 of Edinburgh Ethical Review Committee. The relevant Home Office project licences are P1351480E
348 and 60/4407, and the use of genetically modified organisms approved by local committee reference
349 SBMS 13_007.

350

351 **Competing Financial Interests**

352 The authors declare no competing financial interests in this study.

353

354 **Supplementary Material:**

355 *Figure Supplements:*

356 Figure 1–figure supplement 1a-h
357 Figure 3–figure supplement 1a-c
358
359 *Source Data:*
360 Figure 1–source data 1. Data relating to Figure 1b
361 Figure 1–source data 2. Data relating to Figure 1d
362 Figure 1–source data 3. Data relating to Figure 1f
363 Figure 1–source data 4. Data relating to Figure 1–figure supplement 1a
364 Figure 1–source data 5. Data relating to Figure 1–figure supplement 1f
365 Figure 1–source data 6. Data relating to Figure 1–figure supplement 1h
366 Figure 2–source data 1. Data relating to Figure 2a
367 Figure 2–source data 2. Data relating to Figure 2b
368 Figure 2–source data 3. Data relating to Figure 2c
369 Figure 2–source data 4. Data relating to Figure 2d
370 Figure 2–source data 5. Data relating to Figure 2e-g
371 Figure 3–source data 1. Data relating to Figure 3a
372 Figure 3–source data 2. Data relating to Figure 3e
373 Figure 3–source data 3. Data relating to Figure 3f
374 Figure 3–source data 4. Data relating to Figure 3–figure supplement 1a
375 Figure 3–source data 5. Data relating to Figure 3–figure supplement 1b

376
377

378

References

- 379 1 Choi, D. W. Glutamate neurotoxicity and diseases of the nervous system. *Neuron* **1**, 623-
380 634,(1988).
- 381 2 Lipton, S. A. & Rosenberg, P. A. Excitatory amino acids as a final common pathway for
382 neurologic disorders. *The New England Journal of Medicine* **330**, 613-621,(1994).
- 383 3 Berliocchi, L., Bano, D. & Nicotera, P. Ca²⁺ signals and death programmes in neurons.
384 *Philos Trans R Soc Lond B Biol Sci* **360**, 2255-2258,(2005).
- 385 4 Lau, A. & Tymianski, M. Glutamate receptors, neurotoxicity and neurodegeneration. *Pflugers*
386 *Arch* **460**, 525-542,(2010).
- 387 5 Hardingham, G. E. & Lipton, S. A. Regulation of Neuronal Oxidative and Nitrosative Stress
388 by Endogenous Protective Pathways and Disease Processes. *Antioxid Redox Signal*,(2011).
- 389 6 Parsons, M. P. & Raymond, L. A. Extrasynaptic NMDA receptor involvement in central
390 nervous system disorders. *Neuron* **82**, 279-293,(2014).
- 391 7 Tu, S., Okamoto, S., Lipton, S. A. & Xu, H. Oligomeric Aβ-induced synaptic dysfunction in
392 Alzheimer's disease. *Mol Neurodegener* **9**, 48,(2014).
- 393 8 Furukawa, H., Singh, S. K., Mancusso, R. & Gouaux, E. Subunit arrangement and function
394 in NMDA receptors. *Nature* **438**, 185-192,(2005).
- 395 9 Monyer, H., Burnashev, N., Laurie, D. J., Sakmann, B. & Seeburg, P. H. Developmental and
396 regional expression in the rat brain and functional properties of four NMDA receptors.
397 *Neuron* **12**, 529-540,(1994).

- 398 10 Cull-Candy, S., Brickley, S. & Farrant, M. NMDA receptor subunits: diversity, development
399 and disease. *Curr Opin Neurobiol* **11**, 327-335,(2001).
- 400 11 Traynelis, S. F. *et al.* Glutamate receptor ion channels: structure, regulation, and function.
401 *Pharmacol Rev* **62**, 405-496,(2010).
- 402 12 Paoletti, P. Molecular basis of NMDA receptor functional diversity. *Eur J Neurosci* **33**, 1351-
403 1365,(2011).
- 404 13 Wyllie, D. J., Livesey, M. R. & Hardingham, G. E. Influence of GluN2 subunit identity on
405 NMDA receptor function. *Neuropharmacology* **74**, 4-17,(2013).
- 406 14 Martel, M. A. *et al.* The subtype of GluN2 C-terminal domain determines the response to
407 excitotoxic insults. *Neuron* **74**, 543-556,(2012).
- 408 15 Ryan, T. J., Emes, R. D., Grant, S. G. & Komiyama, N. H. Evolution of NMDA receptor
409 cytoplasmic interaction domains: implications for organisation of synaptic signalling
410 complexes. *BMC neuroscience* **9**, 6,(2008).
- 411 16 Ryan, T. J. *et al.* Evolution of GluN2A/B cytoplasmic domains diversified vertebrate synaptic
412 plasticity and behavior. *Nat Neurosci* **16**, 25-32,(2013).
- 413 17 Frank, R. A. *et al.* NMDA receptors are selectively partitioned into complexes and
414 supercomplexes during synapse maturation. *Nat Commun* **7**, 11264,(2016).
- 415 18 Tymianski, M. Emerging mechanisms of disrupted cellular signaling in brain ischemia. *Nat*
416 *Neurosci* **14**, 1369-1373,(2011).
- 417 19 Tu, W. *et al.* Dapk1 interaction with NMDA receptor NR2B subunits mediates brain damage
418 in stroke. *Cell* **140**, 222-234,(2010).
- 419 20 Lai, T. W., Zhang, S. & Wang, Y. T. Excitotoxicity and stroke: identifying novel targets for
420 neuroprotection. *Prog Neurobiol* **115**, 157-188,(2014).
- 421 21 Bayer, K. U., De Koninck, P., Leonard, A. S., Hell, J. W. & Schulman, H. Interaction with the
422 NMDA receptor locks CaMKII in an active conformation. *Nature* **411**, 801-805,(2001).
- 423 22 Mao, L. M., Jin, D. Z., Xue, B., Chu, X. P. & Wang, J. Q. Phosphorylation and regulation of
424 glutamate receptors by CaMKII. *Sheng Li Xue Bao* **66**, 365-372,(2014).
- 425 23 Husi, H., Ward, M. A., Choudhary, J. A., Blackstock, W. P. & Grant, S. G. N. Proteomic
426 analysis of NMDA receptor-adhesion protein signaling complexes. *Nature Neuroscience* **3**,
427 661-669,(2000).
- 428 24 Collins, M. O. *et al.* Molecular characterization and comparison of the components and
429 multiprotein complexes in the postsynaptic proteome. *J Neurochem* **97 Suppl 1**, 16-
430 23,(2006).
- 431 25 Yoshimura, Y. *et al.* Molecular constituents of the postsynaptic density fraction revealed by
432 proteomic analysis using multidimensional liquid chromatography-tandem mass
433 spectrometry. *J Neurochem* **88**, 759-768,(2004).
- 434 26 Li, K. W. *et al.* Proteomics analysis of rat brain postsynaptic density. Implications of the
435 diverse protein functional groups for the integration of synaptic physiology. *J Biol Chem* **279**,
436 987-1002,(2004).
- 437 27 Jordan, B. A. *et al.* Identification and verification of novel rodent postsynaptic density
438 proteins. *Mol Cell Proteomics* **3**, 857-871,(2004).
- 439 28 Peng, J. *et al.* Semiquantitative proteomic analysis of rat forebrain postsynaptic density
440 fractions by mass spectrometry. *J Biol Chem* **279**, 21003-21011,(2004).
- 441 29 Cheng, D. *et al.* Relative and absolute quantification of postsynaptic density proteome
442 isolated from rat forebrain and cerebellum. *Mol Cell Proteomics* **5**, 1158-1170,(2006).
- 443 30 Bayes, A. *et al.* Characterization of the proteome, diseases and evolution of the human
444 postsynaptic density. *Nat Neurosci* **14**, 19-21,(2011).
- 445 31 Jalan-Sakrikar, N., Bartlett, R. K., Baucum, A. J., 2nd & Colbran, R. J. Substrate-selective
446 and calcium-independent activation of CaMKII by alpha-actinin. *J Biol Chem* **287**, 15275-
447 15283,(2012).

- 448 32 Jia, J. M., Zhao, J., Hu, Z., Lindberg, D. & Li, Z. Age-dependent regulation of synaptic
449 connections by dopamine D2 receptors. *Nat Neurosci* **16**, 1627-1636,(2013).
- 450 33 Castillo, C. *et al.* The N-methyl-D-aspartate-evoked cytoplasmic calcium increase in adult rat
451 dorsal root ganglion neuronal somata was potentiated by substance P pretreatment in a
452 protein kinase C-dependent manner. *Neuroscience* **177**, 308-320,(2011).
- 453 34 Dong, Y. N., Wu, H. Y., Hsu, F. C., Coulter, D. A. & Lynch, D. R. Developmental and cell-
454 selective variations in N-methyl-D-aspartate receptor degradation by calpain. *J Neurochem*
455 **99**, 206-217,(2006).
- 456 35 Gascon, S., Sobrado, M., Roda, J. M., Rodriguez-Pena, A. & Diaz-Guerra, M. Excitotoxicity
457 and focal cerebral ischemia induce truncation of the NR2A and NR2B subunits of the NMDA
458 receptor and cleavage of the scaffolding protein PSD-95. *Mol Psychiatry* **13**, 99-114,(2008).
- 459 36 Hardingham, G. E. & Bading, H. Synaptic versus extrasynaptic NMDA receptor signalling:
460 implications for neurodegenerative disorders. *Nat Rev Neurosci* **11**, 682-696,(2010).
- 461 37 Barria, A. & Malinow, R. NMDA receptor subunit composition controls synaptic plasticity by
462 regulating binding to CaMKII. *Neuron* **48**, 289-301,(2005).
- 463 38 Halt, A. R. *et al.* CaMKII binding to GluN2B is critical during memory consolidation. *EMBO J*
464 **31**, 1203-1216,(2012).
- 465 39 Bano, D. & Nicotera, P. Ca²⁺ signals and neuronal death in brain ischemia. *Stroke; a journal*
466 *of cerebral circulation* **38**, 674-676,(2007).
- 467 40 Duchen, M. R. Mitochondria, calcium-dependent neuronal death and neurodegenerative
468 disease. *Pflugers Arch* **464**, 111-121,(2012).
- 469 41 Nakamura, T. & Lipton, S. A. Redox modulation by S-nitrosylation contributes to protein
470 misfolding, mitochondrial dynamics, and neuronal synaptic damage in neurodegenerative
471 diseases. *Cell Death Differ* **18**, 1478-1486,(2011).
- 472 42 Bell, K. F. & Hardingham, G. E. CNS Peroxiredoxins and Their Regulation in Health and
473 Disease. *Antioxid Redox Signal*,(2011).
- 474 43 Panayotis, N., Karpova, A., Kreutz, M. R. & Fainzilber, M. Macromolecular transport in
475 synapse to nucleus communication. *Trends Neurosci* **38**, 108-116,(2015).
- 476 44 Bell, K. F., Fowler, J. H., Al-Mubarak, B., Horsburgh, K. & Hardingham, G. E. Activation of
477 Nrf2-regulated glutathione pathway genes by ischemic preconditioning. *Oxid Med Cell*
478 *Longev* **2011**, 689524,(2011).
- 479 45 Baxter, P. S., Martel, M. A., McMahon, A., Kind, P. C. & Hardingham, G. E. Pituitary
480 adenylate cyclase-activating peptide induces long-lasting neuroprotection through the
481 induction of activity-dependent signaling via the cyclic AMP response element-binding
482 protein-regulated transcription co-activator 1. *J Neurochem* **118**, 365-378,(2011).
- 483 46 Bading, H., Ginty, D. D. & Greenberg, M. E. Regulation of gene expression in hippocampal
484 neurons by distinct calcium signaling pathways. *Science* **260**, 181-186,(1993).
- 485 47 Papadia, S., Stevenson, P., Hardingham, N. R., Bading, H. & Hardingham, G. E. Nuclear
486 Ca²⁺ and the cAMP response element-binding protein family mediate a late phase of
487 activity-dependent neuroprotection. *J Neurosci* **25**, 4279-4287,(2005).
- 488 48 Bell, K. F. *et al.* Mild oxidative stress activates Nrf2 in astrocytes, which contributes to
489 neuroprotective ischemic preconditioning. *Proc Natl Acad Sci U S A* **108**, E1-2; author reply
490 E3-4,(2011).
- 491 49 Bell, K. F. *et al.* Neuronal development is promoted by weakened intrinsic antioxidant
492 defences due to epigenetic repression of Nrf2. *Nat Commun* **6**, 7066,(2015).
- 493 50 Puddifoot, C. *et al.* PGC-1alpha negatively regulates extrasynaptic NMDAR activity and
494 excitotoxicity. *J Neurosci* **32**, 6995-7000,(2012).
- 495 51 Hardingham, N. R., Hardingham, G. E., Fox, K. D. & Jack, J. J. Presynaptic efficacy directs
496 normalization of synaptic strength in layer 2/3 rat neocortex after paired activity. *J*
497 *Neurophysiol* **97**, 2965-2975,(2007).

498 52 Baxter, P. S. *et al.* Synaptic NMDA receptor activity is coupled to the transcriptional control
499 of the glutathione system. *Nat Commun* 6, 6761,(2015).

500

501

502

Figure Legends

503

504 **Figure 1. Neither Dapk1 nor excitotoxic insults increase GluN2B phosphorylation on Ser-**

505 **1303. A,B)** Strong excitotoxic insults induce GluN2B Ser-1303 dephosphorylation at later

506 timepoints. Western analysis of extracts from cortical neurons treated as indicated with NMDA or
507 bicuculline (50 μ M) plus 4-amino pyridine (250 μ M). (F(2,24)=3.904, P=0.034 (Two-way ANOVA).

508 *P= 0.0053 (Sidak's post-hoc test; 95% CI of diff: 0.1777 to 1.139, comparison to control without
509 NMDA treatment, N=3). **C,D)** Mimicking ischemic conditions triggers dephosphorylation of GluN2B

510 Ser-1303 in an NMDAR-dependent manner. Oxygen-glucose deprivation (OGD) applied for 120 min
511 \pm MK-801 (10 μ M). F(1,12)=6.69, P=0.024 (Two-way ANOVA). *P= 0.0003 (Sidak's post-hoc test,

512 95% CI of diff: 0.3289 to 0.9172, N=4). **E,F)** Dapk1 deficiency does not influence basal or NMDA-

513 induced GluN2B Ser-1303 phosphorylation status. Neurons were treated \pm 50 μ M NMDA for 60 min.

514 F(1,10)=345.1, P<0.0001 (Two-way ANOVA, Con vs. NM). *P<0.0001 (both, compared to Con of
515 that genotype, 95% CI of diff: 0.6384 to 0.9342, and 0.6411 to 0.9826 (reading left to right), N=4

516 WT, N=3 KO; with "N" defined as a distinct culture from a distinct animal). ns: F(1,10)=0.5418,

517 P=0.4786.

518

519 **Figure 2. Excitotoxic and ischemic insults are not ameliorated by Dapk1 deficiency. A, B)**

520 NMDA-induced neuronal death is independent of Dapk1. Cortical neurons at DIV10 (A) or DIV16 (B)

521 were treated as indicated for 1 h, with neuronal death assessed at 24 h. The p values relate to a
522 two-way ANOVA test of differences between WT and Dapk^{-/-} neurons (F(1,10) = 0.2676, n=6 WT, 6

523 KO (DIV10); F(1,7)=0.8871, 2-way ANOVA, n=4 WT, 5 KO (DIV16)). For each condition/genotype

524 combination, 800-1000 cells were analysed per biological replicate. **C)** OGD-induced neuronal

525 death is independent of Dapk1. Cortical neurons at DIV10 were subjected to OGD for 120 min,

526 before being returned to control medium. Neuronal death was assessed at 24 h. No genotype-

527 dependent difference was observed (F (1,12)=0.5062, P=0.490, but a strong influence of OGD was

528 observed: F (1,12) = 63.54, P<0.0001, two-way ANOVA. #P=0.0002, 0.0002 (reading left to right);

529 Sidak's post-hoc test comparing control to OGD condition (n=4 WT, n=4 KO). **D)** Dapk1 deficiency

530 does not influence NMDAR currents. NMDAR currents were measured in n=16 WT cells (from 4

531 separate cultures) and n=25 KO cells (from 6 separate cultures). Currents were normalized to the

532 mean current recorded from WT cells recorded on that precise day. P=0.411 (t=0.831, df=39),

533 unpaired t-test. **E-G)** Dapk1 deficiency does not influence vulnerability to ischemia *in vivo*. Adult

534 age-matched mice (n=14 WT; n=16 KO) were subjected to 20 min bilateral common carotid artery

535 occlusion, sacrificed at 3 d, and pathology analysed. CA1/2 (E): P=0.555 (t=0.598, df=28); CA1

536 (F):P=0.572 (t=0.572, df=28), CA2 P=0.592(G, t=0.543, df=28). Scale bar = 50 μ m.

537

538 **Figure 3. Both TAT-NR2B_{CT} and TAT-sNR2Bs_{CT} are direct NMDAR antagonists. A-D)** Both
539 TAT-NR2B_{CT} and TAT-sNR2B_{CT} (scrambled version of TAT-NR2B_{CT}) immediately antagonize
540 NMDAR currents upon extracellular exposure. NMDA-induced currents were recorded under whole-
541 cell voltage clamp, with the indicated peptides (at 5 μ M) applied approximately 5 s after NMDA (to
542 allow NMDAR currents to reach steady state). Arg-rich refers to the arginine-rich positively charged
543 peptide; Neutral refers to the neutral peptide-see main text for sequences of these as well as TAT-
544 NR2B_{CT} and TAT-sNR2B_{CT}. NMDA-induced NMDAR currents were monitored for a further 45 s and
545 the percentage drop in currents calculated, compared to no peptide at all (Con) which represents a
546 measure of natural desensitization over this period. $P < 0.0001$ (one-way ANOVA). * $P < 0.0001$,
547 Sidak's post-hoc test ($n = 8$ of all conditions). Example traces shown in (B) (C) and (D). Scale bar: 15
548 s, 500 pA. **E)** NMDAR antagonism by TAT-NR2B_{CT} is inhibited by Mg^{2+} blockade. NMDAR currents
549 were measured, after which neurons were incubated in TAT-NR2B_{CT} (5 or 0.5 μ M) for 60 s in the
550 presence or absence of 1 mM Mg^{2+} , after which NMDAR currents were measured again (in zero
551 Mg^{2+} , no peptide). $P < 0.0001$ (one-way ANOVA, $F(1,22) = 47.16$ (effect of $[Mg^{2+}]$)). * $P < 0.0001$,
552 $P = 0.0007$, Sidak's post-hoc test (zero Mg^{2+} : $n = 6$ (0.5 μ M), $n = 7$ (5 μ M); 1 mM Mg^{2+} : $n = 6$ (0.5 μ M),
553 $n = 7$ (5 μ M)). **F-H)** NMDAR antagonism by TAT-NR2B_{CT} is more effective on open channels. See
554 main text for experimental details. $P < 0.0001$ (two-way ANOVA, comparing initial current with
555 subsequent measurements: $F(2, 45) = 25.22$. $P < 0.0001$ (two-way ANOVA, comparing 'closed-then-
556 closed' protocol (grey bars, $n = 8$) with 'closed-then-open' protocol (black bars, $n = 9$): $F(1, 45) =$
557 18.26 . # $P = 0.003$, 0.0009 (Sidak's post-hoc test), comparing to initial currents. * $P < 0.0001$ (Sidak's
558 post-hoc tests), comparisons indicated. **(G)** shows example recordings taken during the consecutive
559 "closed" then "closed" channel protocol. **(H)** shows example recordings taken during the
560 consecutive "closed" then "closed" channel protocol. Scale bar = 1 s, 250 pA.

561

562

563

564

565

Figure Supplement Legends

566 **Figure 1–figure supplement 1. A,B)** Neurons were treated with staurosporine (STS, 1 μ M) or FK-
567 506 (FK, 5 μ M) + okadaic acid (OA, 10 μ M) for one hour, after which protein was harvested and
568 western analysis for Phospho- (GluN2B Ser-1303) levels performed. $P = 0.0023$ (1-way ANOVA).
569 Individual P-values left-to-right: 0.026, 0.047 ($n = 8$ (FK+OA); $n = 4$ (STS)). **C)** Schematic depicting the
570 amino-acid changes resulting from mutations of the *Grin2b* gene in the GluN2B ^{Δ CaMKII} allele. **D)**
571 Example Phospho- (GluN2B Ser-1303) western blot illustrating the lack of immunoreactivity of the
572 mutated domain in extracts from GluN2B ^{Δ CaMKII/ Δ CaMKII} neurons. **E,F)** timecourse of GluN2B Ser-1303
573 phosphorylation status in response to NMDA treatment (50 μ M). $F(5,10) = 4.019$, $P = 0.023$ (one-way
574 ANOVA). * $P = 0.041$ (Sidak's post-hoc test ($n = 3$), 95% CI of diff 0.01897 to 1.024). **G,H)** Experiment

575 performed as per Figure 1a except neurons were at DIV16 rather than DIV10. $F(2, 24) = 5.324$,
576 $P=0.0122$ (two-way ANOVA). * $P=0.0022$ (Sidak's post-hoc test ($N=3$)).

577

578

579 **Figure 3–figure supplement 1. A)** Neurons were treated where indicated with 50 μM TAT-NR2B_{CT}
580 for 1 h, with death assessed after 24 h. **B)** Neurons were pre-treated where indicated with TAT-
581 NR2B_{CT} or TAT-sNR2B_{CT} for 1 h, prior to 1h NMDA treatment at the indicated concentrations, in the
582 continued presence of the peptides where used. Subsequently, both NMDA and peptide were
583 removed from the medium and death assessed after a further 23 h. $P<0.0001$ (effect of peptide:
584 two-way ANOVA, $F(2,40)=76.13$, $n=3-4$). * $P= 0.0027$, 0.0039 (20 μM), <0.0001 , <0.0001 (30 μM),
585 <0.0001 , <0.0001 (50 μM), <0.0001 , <0.0001 (100 μM), Sidak's post-hoc test. **C)** Example trace
586 from an experiment where NMDA-induced currents were recorded under whole-cell voltage clamp,
587 with NR2B_{CT}(1292-1304)-TAT (5 μM , Merck Millipore) applied approximately 5 s after NMDA (to
588 allow NMDAR currents to reach steady state). NMDA-induced NMDAR currents were monitored to
589 determine the degree of blockade. The trace is representative of 8 cells recorded this way, with the
590 peptide blocking by $63 \pm 3 \%$. Scale bar = 5 s, 500 pA.

591

592

Source Data Legends

593 **Figure 1–source data 1.** Data relating to Figure 1b

594 **Figure 1–source data 2.** Data relating to Figure 1d

595 **Figure 1–source data 3.** Data relating to Figure 1f

596 **Figure 1–source data 4.** Data relating to Figure 1–figure supplement 1a

597 **Figure 1–source data 5.** Data relating to Figure 1–figure supplement 1f

598 **Figure 1–source data 6.** Data relating to Figure 1–figure supplement 1h

599 **Figure 2–source data 1.** Data relating to Figure 2a

600 **Figure 2–source data 2.** Data relating to Figure 2b

601 **Figure 2–source data 3.** Data relating to Figure 2c

602 **Figure 2–source data 4.** Data relating to Figure 2d

603 **Figure 2–source data 5.** Data relating to Figure 2e-g

604 **Figure 3–source data 1.** Data relating to Figure 3a

605 **Figure 3–source data 2.** Data relating to Figure 3e

606 **Figure 3–source data 3.** Data relating to Figure 3f

607 **Figure 3–source data 4.** Data relating to Figure 3–figure supplement 1a

608 **Figure 3–source data 5.** Data relating to Figure 3–figure supplement 1b

609

610

611

612

613

Figure 1

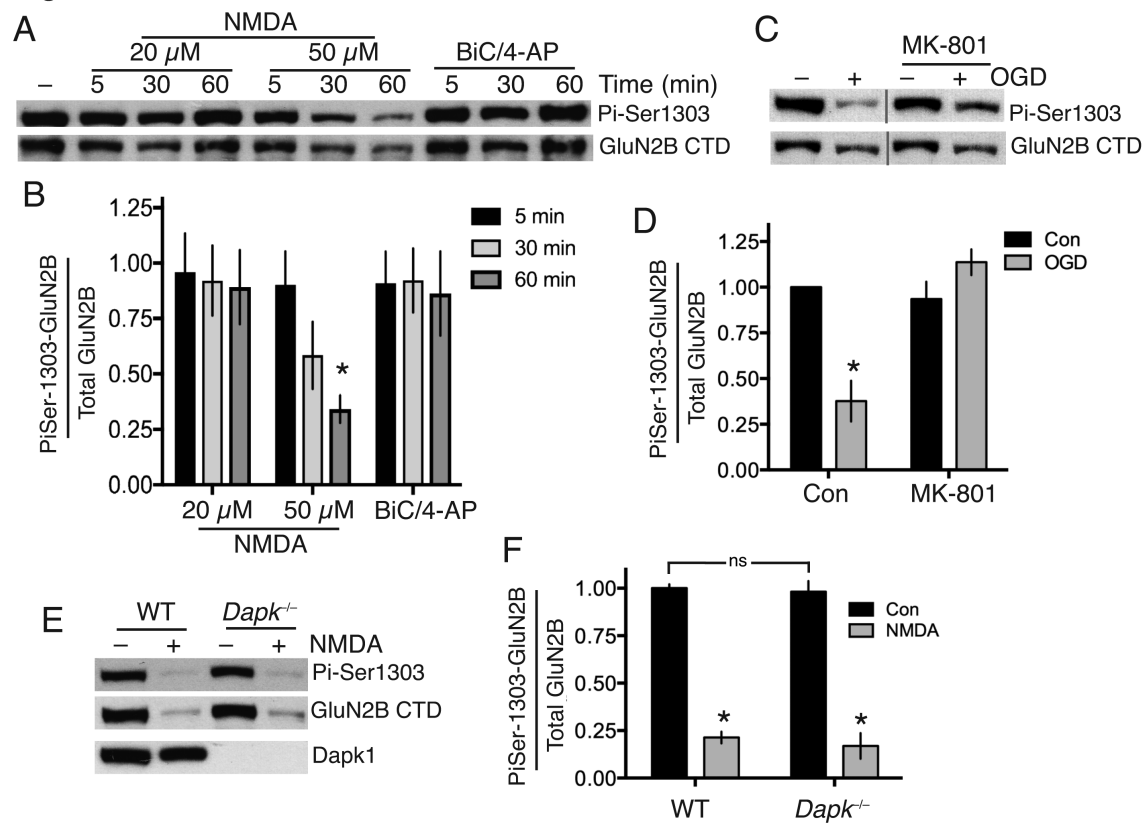


Figure 2

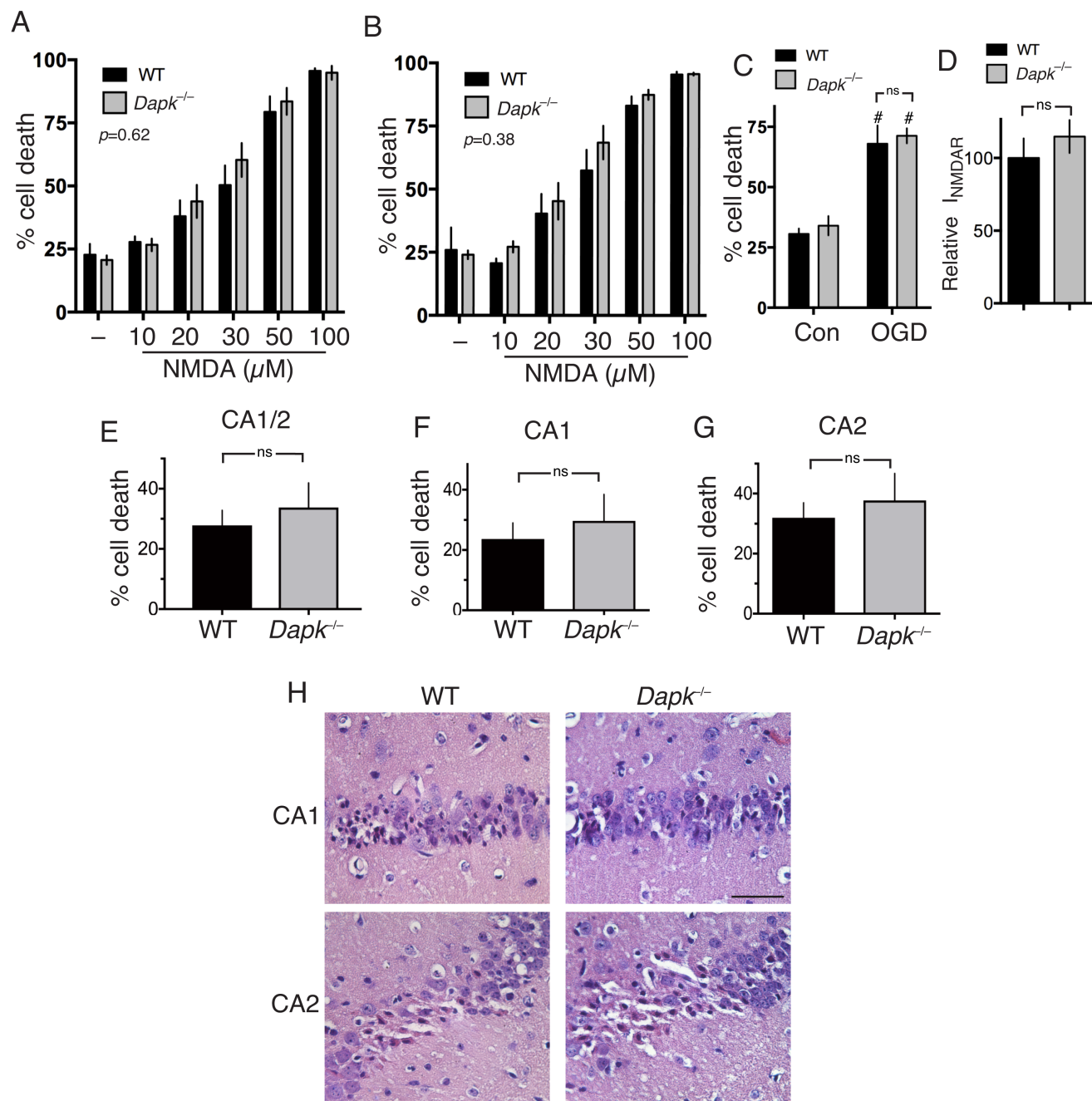


Figure 3

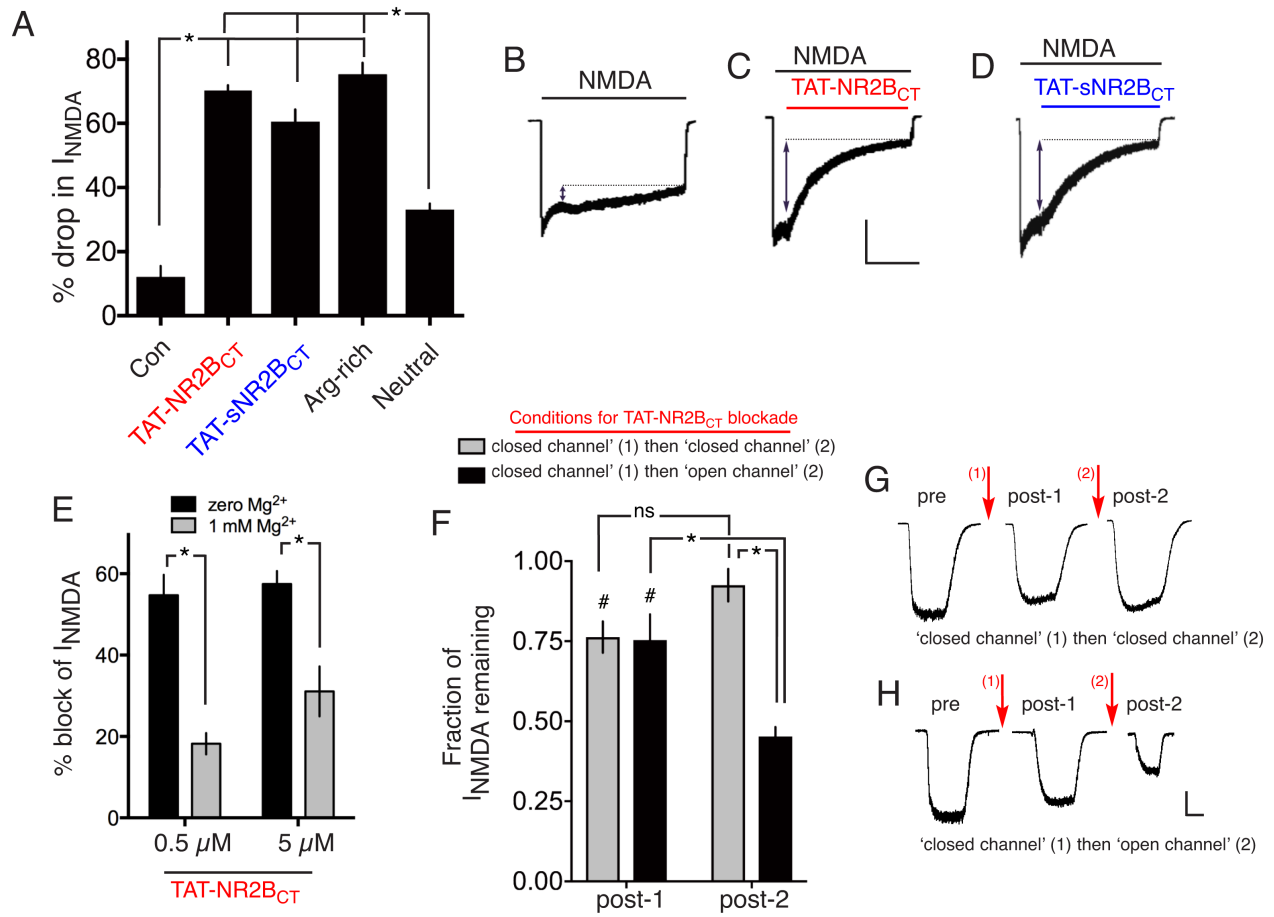


Figure 1–figure supplement 1

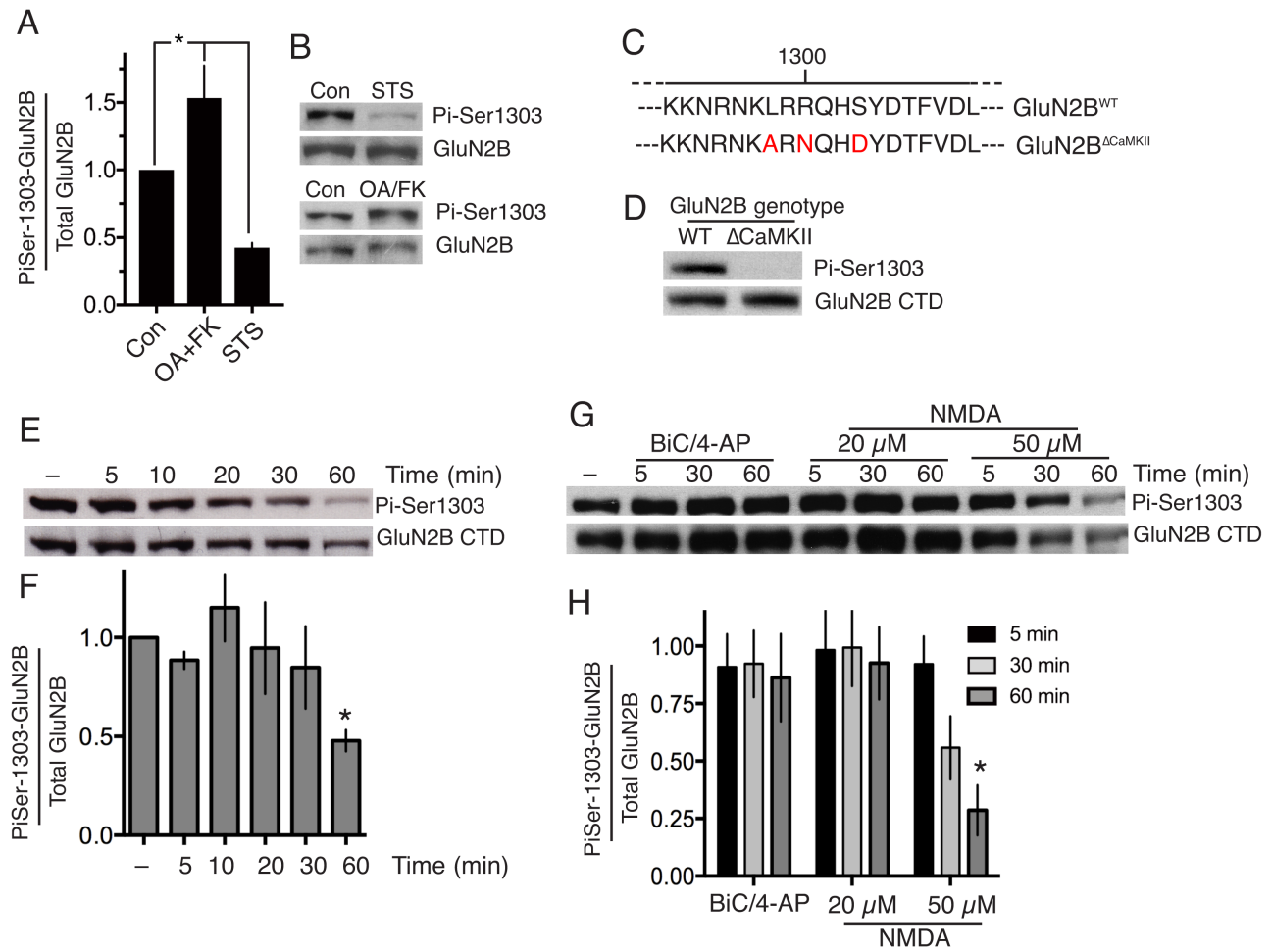


Figure 3–figure supplement 1

